Jurnal Kejuruteraan SI 3(1) 2020: 35-41
https://doi.org/10.17576/jkukm-2020-si3(1)-06

Normalized Polarization Ratio Analysis for ULF Precursor Detection of the 2009 *M*7.6 Sumatra and 2015 *M*6.8 Honshu Earthquakes

Khairul Adib Yusof[a,a2], Mardina Abdullah[a,b]*, Nurul Shazana Abdul Hamid[a,c], Suaidi Ahadi[d] & Akimasa Yoshikawa[e]

[a]*Space Science Centre, Institute of Climate Change, Universiti Kebangsaan Malaysia, Malaysia*
[a2]*Department of Physics, Faculty of Science, Universiti Putra Malaysia, Selangor, Malaysia*
[b]*Department of Electrical, Electronic and Systems Engineering, Faculty of Engineering and Built Environment, Universiti Kebangsaan Malaysia, Malaysia*
[c]*Department of Applied Physics, Faculty of Science and Technology, Universiti Kebangsaan Malaysia, Malaysia*
[d]*Department of Geophysics, Indonesian Agency for Meteorology, Climatology and Geophysics, Jakarta, Indonesia*
[e]*International Centre for Space Weather Science and Education, Kyushu University, Fukuoka, Japan*

**Corresponding author: mardina@ukm.edu.my*

Received 13 December 2019, Received in revised form 12 March 2020
Accepted 15 April 2020, Available online 30 September 2020

ABSTRACT

The utilization of geomagnetic field data especially in the ultra-low frequency range has been shown by prior studies to have the potential to detect earthquake precursors. The most widely used signal processing method for this purpose is arguably the polarization ratio analysis. In this paper, the method was improved by introducing a new normalization process with dissimilar ranges for the vertical and horizontal components. The normalized method was applied to geomagnetic field data that were recorded at locations near the earthquakes which had occurred in Sumatra, Indonesia on 30th September 2009 (M7.6) and Honshu, Japan on 12th May 2015 (M6.8) to evaluate the method's reliability and effectiveness in two different regions, i.e., the equatorial and mid-latitudinal regions. The results showed that the precursors obtained from the normalized method were less disturbed by random fluctuations and had more distinguishable amplitudes compared to the non-normalized classic method in both studied regions.

Keywords: Earthquake precursor; Geomagnetic ULF; Normalized polarization ratio

INTRODUCTION

The immense destruction and fatalities resulting from earthquakes has spurred the development of earthquake forecasting on a global scale. The short-term forecasting, which provides warnings a week to a month before earthquakes, is the most useful because of its higher reliability compared to the long- and medium-term forecasting (Hayakawa, 2015). The current limited capability of seismometers in measuring microfracture formation and minor ground movement during the earthquake preparation phase has shifted researchers' interest to non-seismological approaches. One of the most popular approaches is the detection of anomalous geomagnetic emission.

The exact mechanism of the geomagnetic emission generation by underground seismic activities has not been determined and is not well-understood. However, prior studies have proposed several possible mechanisms including (1) piezomagnetic or piezoelectric effects (Dudkin et al. 2010), (2) electrification during microfracturing process (Molchanov and Hayakawa, 1995), and (3) induced electric current because of changes in underground conductivity (Chauhan et al. 2012).

Geomagnetic emission in the ultra-low frequency (ULF) range has the greatest potential for the detection of earthquake precursor. This is because such emission is able to propagate through lithospheric layer of the earth with minimal attenuation. The ability is due to the low-pass filter nature of the lithosphere that only damps high-frequency components (Chauhan et al. 2012). Prior studies have successfully demonstrated that the ULF range within 0.01 – 0.1 Hz is the most appropriate for this purpose (Chen et al. 2015; Rawat et al. 2016; Yusof et al. 2019b).

Despite the advantageous ability, the detection of seismogenic (i.e., earthquake-related) ULF emission is practically problematic. Not only is the intensity very weak (around 1 nT) but it is also usually obscured by the more intense natural background geomagnetic field (Zelinskiy et al. 2014). In order to distinguish between the emission and the background, several studies have applied the polarization ratio analysis which essentially separates the vertical component of the geomagnetic field from the horizontal component (Currie and Waters 2014; Yusof et al. 2019a). The main principle of this method of analysis is that underground emission generated by local crustal activity would affect only the vertical component, while

the horizontal component is mainly influenced by global magnetospheric currents (Hirano and Hattori 2011).

Since its first introduction by Hayakawa et al. (1996), the polarization ratio analysis has been improved over the decades. One of the notable attempts was the implementation of a normalization process by Ida et al. (2008). In their work, a z-score normalization process was introduced where both vertical and horizontal component were normalized by using the following formula:

$$X_{norm} = \frac{X - \mu_X}{\sigma_X} \quad (1)$$

where X and X_{norm} are the original and the normalized field components respectively, μ_X is the mean and σ_X is the standard deviation. The normalized method was successful in detecting the precursor of the 2003 M 6.0 Kashi, China earthquake.

Despite their success, the same results have not been reproduced with other earthquakes. Preliminary analysis of our current study (not shown here) using this type of normalization was also unsuccessful in discerning any precursory anomalies prior to our studied earthquakes. Thus, it is possible that their success was event specific. This urges for a more effective normalized polarization ratio analysis. A different type of normalization, for example by a range of values, could be considered. By using this type of normalization, the minimum and maximum values of the actual data are reassigned into new values, hence modifying all the values in between.

The implementation of the analysis method on earthquakes in different regions could be beneficial to evaluate its global reproducibility. Two strong-to-major past earthquakes, which were recorded in Sumatra, Indonesia on 30th September 2009 (EQ1) and Honshu, Japan on 12th May 2015 (EQ2) were considered appropriate for this purpose as they represent earthquakes in the equatorial and mid-latitudinal regions, respectively. Both earthquakes are considered mainshocks in their respective sequence of earthquakes. Details of the earthquakes are listed in Table 1.

In this study, we implemented the non-normalized classic polarization ratio analysis as an attempt to detect ULF geomagnetic precursor of both earthquakes (i.e., EQ1 and EQ2). Based on the outcomes, a new normalization process was developed to improve the analysis method in terms of reliability and effectiveness. The results obtained from these methods of analysis were then compared to evaluate their performance.

METHODOLOGY

INSTRUMENTATION AND DATA

The geomagnetic field was the primary data utilized in this study which was acquired from the Magnetic Data Acquisition System (MAGDAS) project. This project is operated by the International Center for Space Weather Science and Education (ICSWSE), Kyushu University, Japan. Their magnetometers are the ring-core fluxgate type which record the ambient geomagnetic field intensity (unit: nanotesla, nT) in three components, namely the magnetic northward (H), the magnetic eastward (D) and the downward vertical (Z) (Yumoto and MAGDAS Group, 2007). In this study, 1-Hz data starting from 45 days before until 15 days after the mainshocks were obtained for the Kotatabang, Indonesia (KTB) and Tohno, Japan (TNO) MAGDAS stations. Details of the stations are listed in Table 1.

Two mainshock events, which will later be referred separately as EQ1 and EQ2, were selected for this study as shown in Figure 1. As illustrated in the figure, the Sicincin (SCN) station was actually nearer to EQ1; however, the station went offline during the observation period causing data unavailability. It is important to note that in addition to the two mainshocks, there were other earthquakes with smaller magnitudes (foreshocks and aftershocks) occurring close to each other spatially and temporally. However, only the mainshocks were the focus of this study since they had the largest magnitudes in each region and occurred reasonably close to the observatory stations. Both mainshocks were determined to be 'detectable' based on their magnitudes, M and epicentral distances, d (i.e., the distance between the earthquake epicenter and the observatory station). The term 'detectable' in this context refers to an earthquake with a magnitude of M that would produce ULF emission that is sufficiently strong enough to be detected by a nearby station if its epicentral distance is within its maximum detectable distance, d_{det} as given by Hayakawa (2015):

$$d_{det} = \frac{M - 4.5}{0.025} \quad (2)$$

The constants in Equation (2) were derived empirically from multiple case studies carried out previously. It was determined that d_{det} for EQ1 and EQ2 were 124 km and 92 km respectively, which were greater than their actual d (refer Table 1).

In order to calculate the seismicity impact of the earthquakes on the respective observatory stations, Molchanov & Hayakawa (2008) introduced the local seismicity index (K_{LS}), which is computed as follows:

$$K_{LS} = \frac{10^{0.75M}}{d + 100} \quad (3)$$

The calculated index values for both earthquakes are also included in Table 1.

During heightened solar activity levels, events such as solar flares, geomagnetic storms and high-speed solar wind ejections may occur; these periods are known as disturbed days. On these days, geomagnetic field data are typically affected in the form of high amplitude disturbances which can mistakenly be perceived as anomalies. Therefore, geomagnetic indices which indicate the global geomagnetic activity level need to be observed to distinguish earthquake-origin signatures from solar-terrestrial disturbances.

In this study, the disturbance storm time (Dst) and planetary (ap) indices are appropriate for the purpose since

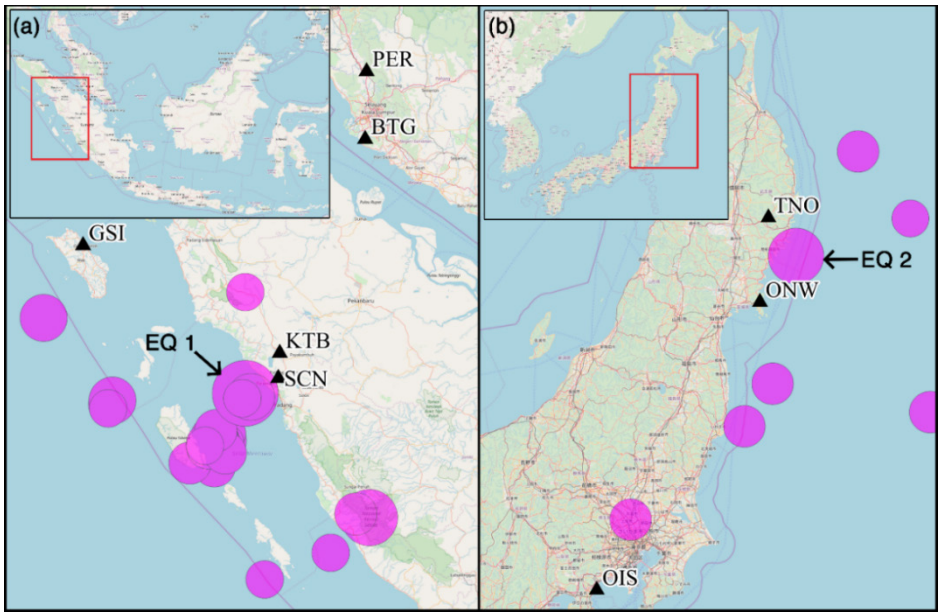

FIGURE 1. Maps of (a) Sumatra, Indonesia, and (b) Honshu, Japan. The black triangles are the installed MAGDAS stations, the magenta circles represent the earthquakes that occurred during the observation period where their radii are proportional to the magnitudes. Mainshocks (EQ1 and EQ2) are pointed by the arrows.

TABLE 1. Details of the MAGDAS stations and properties of the studied earthquakes

Station code	Station coordinate	EQ	Date (UTC)	Coordinate	M	h (km)	d (km)	d_{det} (km)	K_{LS}
KTB	-0.20° N, 100.32° E	1	30/09/2009	-00.76° N, 99.84° E	7.6	80	82	124	2754
TNO	39.37° N, 141.60° E	2	12/05/2015	38.95° N, 141.99° E	6.8	40	58	92	799

they were measured by multiple observatory stations in the equatorial and the mid-latitudinal regions, respectively (Rostoker 1972). Both indices were sampled every 3 hours in the unit of nT. Values of $Dst < -50$ nT and $ap > 50$ nT indicate disturbed days; thus, anomalies on these days should be disregarded as earthquake precursors (Hasbi et al. 2011).

CLASSIC POLARIZATION RATIO ANALYSIS

The classic polarization ratio analysis method is based on the observation of a daily precursory parameter called $P_{Z/G}$, which is the ratio of power spectral density (PSD) of the vertical, $S_Z(f)$ to PSD of total horizontal field components, $S_G(f)$ calculated using Equation (4). The total horizontal field, G was calculated first, where $G = \sqrt{H^2 + D^2}$.

$$P_{Z/G}(f) = \frac{S_Z(f)_{\Delta f}}{S_G(f)_{\Delta f}} \tag{4}$$

In Equation (4), the Δ operator indicates the averaging of PSD value over the frequency range of Δf . We observed nine narrowband frequency ranges between 0.01 – 0.10, which were Δf = 0.01 – 0.02, 0.02 – 0.03, …, 0.09 – 0.10 Hz.

It is typical in this kind of analysis that a shorter night local time (LT) period (22:00 – 02:00 LT) of geomagnetic field data is observed rather than the whole 24-hours data to represent one day $P_{Z/G}$ value. This is to minimize man-made noise which is usually elevated during the daytime specifically between 07:00 – 17:00 LT (Serita et al. 2005). In order to consider an increment of $P_{Z/G}$ in a given day of i as significantly anomalous in terms of statistics, its value needs to exceed two standard deviations (σ) from the mean (μ) of the whole observation period:

$$P_{Z/G,i} > \mu + 2\sigma \tag{5}$$

NORMALIZED POLARIZATION RATIO ANALYSIS

Based on the same central idea, we proposed an improvement of the classic polarization ratio analysis method by normalizing the values of S_Z and S_G to certain ranges, as opposed to z -score normalization as introduced by Ida et al. (2008). The general formula of range normalization is as follows:

$$S_{X,norm} = \left(S_X - S_{X,max}\right)\left(\frac{M-m}{S_{X,max} - S_{X,min}}\right) + M \tag{6}$$

In the formula, X can be either G (horizontal) or Z (vertical) components, $S_{X,norm}$ and S_X are the normalized and original daily value of PSD of component X respectively, while $S_{X,min}$ and $S_{X,max}$ refer to the minimum and maximum values of PSD of component X throughout the period of observation. The terms m and M are the lower and upper boundaries of the selected range, respectively; they are written as [m, M] for the rest of this paper. The

calculated normalized PSD values ($S_{G,norm}$ and $S_{Z,norm}$) were plugged in Equation (4) to calculate $P_{Z/G}(f)$ parameter. Note that the f values are the same as the ones used in the classic method.

Through trial and error (results are not shown), we found that the normalization by the following ranges were the most effective in detecting precursory anomalies: [1, 2] for S_G and [1, 3] for S_Z. The combination of the range values is effective because it (1) avoids any daily value of S_G being 0, thus avoiding infinitely high $P_{Z/G}$, and (2) gives S_Z a higher proportion in determining the value of the corresponding $P_{Z/G}$ since Z is the most affected component because of crustal activities. We also established a second condition to consider $P_{Z/G}$ as anomalous in addition to the one mentioned in Equation (5), that is $P_{Z/G,i}$ must be greater than 1.5. This threshold value comes from the simple division of the maximum value of normalized S_Z (i.e., 3) over maximum S_G (i.e., 2). In actuality, during the preparatory phase of earthquakes, the value of S_G may drop to lower than 2 which causes a much higher value of $P_{Z/G}$.

RESULTS AND DISCUSSION

CLASSIC POLARIZATION RATIO ANALYSIS

We present the results of the classic polarization ratio analysis for EQ1 and EQ2 in this section. In Figure 2(a) and Figure 3(a), the magenta triangles represent every earthquake located less than 200 km from the respective MAGDAS stations; the color-filled triangles correspond to EQ1 and EQ2. The red shades in both figures indicate disturbed periods where either *Dst* or *ap* indices exceeded the respective disturbed day thresholds (blue and red dashed lines in the figures). As has been established, any anomalous $P_{Z/G}$ values during these periods were ignored.

Based on Figure 2(b), 2(c) and 2(d), it is apparent that $P_{Z/G}$ of EQ1 in ranges between 0.01 – 0.05 (comprising 0.01 – 0.02, 0.02 – 0.03, 0.03 – 0.04 and 0.04 – 0.05) and 0.06 – 0.09 Hz exceeded the respective $\mu+2\sigma$ thresholds (dashed lines) several times throughout the observation period, but the excesses were minimal. Therefore, we paid attention to the high $P_{Z/G}$ value of 2.33 in 0.04 – 0.05 Hz (Figure 2(c)) on 8th September (inside the magenta circle) which possibly was the precursor of the mainshock on 30th September 2009. However, this frequency range also showed several fluctuations which nearly reached the threshold value three times before and two times after the earthquake. This behavior of precursory parameter leads to significant ambiguity where the real precursor cannot be clearly distinguished from the random fluctuations.

In Figure 3(b), 3(c) and 3(d), the overall values of $P_{Z/G}$ of EQ2 in all frequency ranges were relatively low, where the highest value was only 0.83 that was observed in 0.05 – 0.06 Hz (Figure 3(c)) on 6th May 2015, which was a disturbed day. By ignoring anomalies during disturbed days and other random fluctuations, we focused on the high and threshold-exceeding daily value of 0.59 in 0.03 – 0.04 Hz (Figure 3(b)) on 29th April 2015 (inside the magenta circle). Similar to the observation in Figure 2(c), there existed several notable fluctuations before and after the earthquake.

Although the anomalies on 8th September 2009 and 29th April 2015 might be the precursors to EQ1 and EQ2 respectively, we assert that the reliability and effectiveness of $P_{Z/G}$ parameter could be further improved. In this context, reliability is indicated only by having a precursor appearing before an earthquake event which would essentially eliminate ambiguity. Meanwhile, effectiveness specifies that the precursor has a very distinctive feature (e.g., high amplitude relative to the background values) that eases precursor identification.

NORMALIZED POLARIZATION RATIO ANALYSIS

In this section, the normalized polarization ratio analysis results are presented. The contents in Figure 4(a) and Figure 5(a) are identical to Figure 2(a) and Figure 3(a), respectively.

The preliminary observation of normalized $P_{Z/G}$ in all nine frequency ranges were carried out similar to the classic method; however, they are not shown here. Instead, we only focused on one frequency range that had a daily value that was considered anomalous, and had the highest amplitude compared to other frequency ranges.

By referring to Figure 4(b), it was found that the range of 0.08 – 0.09 Hz had an apparent anomaly on 26th September 2009 (4 days before EQ1) with an amplitude of 2.20 (inside the magenta circle). It is acknowledged that there was a slight increment on 10th September 2009; however, its amplitude was 1.43, which did not satisfy the second condition of being a precursor. Other than that, the values of $P_{Z/G}$ remained consistently low throughout the period.

On the other hand, for EQ2, the range of 0.03 – 0.04 contained the probable anomaly, hence the one included in Figure 5(b). From the figure, it is shown that the normalized $P_{Z/G}$ was significantly high during two of the six disturbed periods (shaded red, *ap* index exceeded 50 nT). In addition to this, the parameter was also high on 4th May 2015 (8 days before EQ2) with an amplitude of 2.38 (inside the magenta circle). No other anomalous increment was observed throughout the period.

Table 2 compares the characteristics of the observed anomalies obtained from the two analysis methods. We would like to comment on the dissimilarity of the dates of the anomaly appearance when the different methods were used. This resulted in different lead times (i.e., the difference in days between the appearance of precursory anomalies and the occurrence of the mainshock), where the classic method yielded significantly longer lead times (i.e., 22 and 13 days) compared to the normalized method (i.e., 4 and 8 days). Even though long lead times (more than a week) are not impossible, most previous studies reported lead times of around a week or less (Chauhan et al. 2012; Ida et al. 2008; Takla et al. 2011). It is also worth noting that the classic method revealed a larger amplitude anomaly

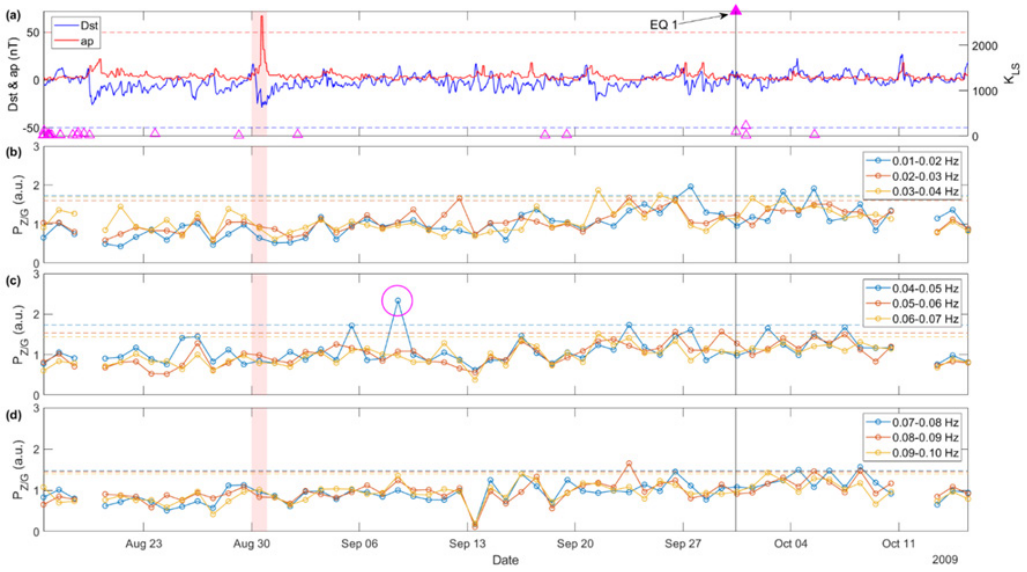

FIGURE 2. Classic polarization ratio analysis results for EQ1. The figure shows temporal evolutions of (a) Dst and ap indices (left) and K_{LS} of earthquakes (right), (b) $P_{Z/G}$ in 0.01 – 0.04 Hz, (c) in 0.04 – 0.07 Hz, and (d) in 0.07 – 0.10 Hz. Dashed lines in (a) are the disturbed day thresholds, while in (b) – (d), they are the $\mu + 2\sigma$ thresholds.

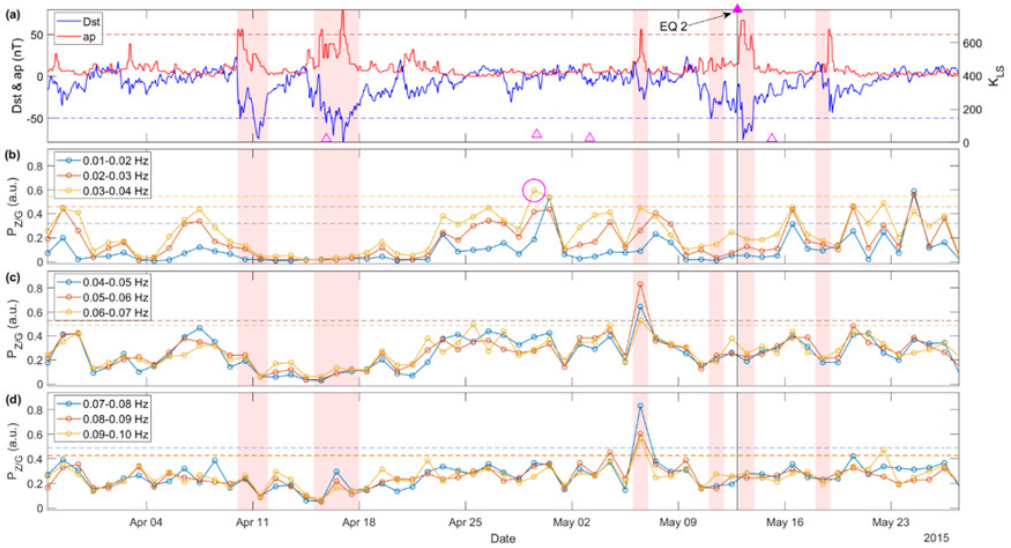

FIGURE 3. Classic polarization ratio analysis results for EQ2. The figure shows temporal evolutions of (a) Dst and ap indices (left) and K_{LS} of earthquakes (right), (b) $P_{Z/G}$ in 0.01 – 0.04 Hz, (c) in 0.04 – 0.07 Hz, and (d) in 0.07 – 0.10 Hz. Dashed lines in (a) are the disturbed day thresholds, while in (b) – (d), they are the $\mu + 2\sigma$ thresholds.

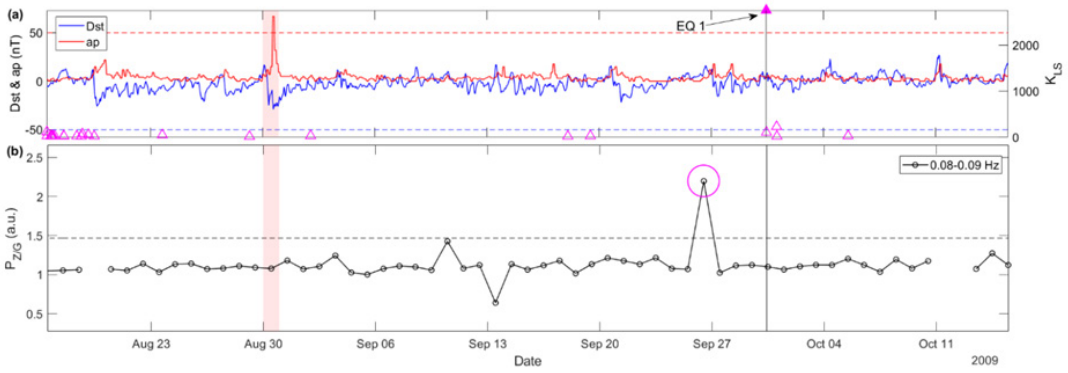

FIGURE 4. Normalized polarization ratio analysis results for EQ1. The figure shows temporal evolutions of (a) Dst and ap indices (left) and K_{LS} of earthquakes (right), and (b) $P_{Z/G}$ in 0.08 – 0.09 Hz. Dashed lines in (a) are the disturbed day thresholds, while in (b), they are the $\mu + 2\sigma$ threshold.

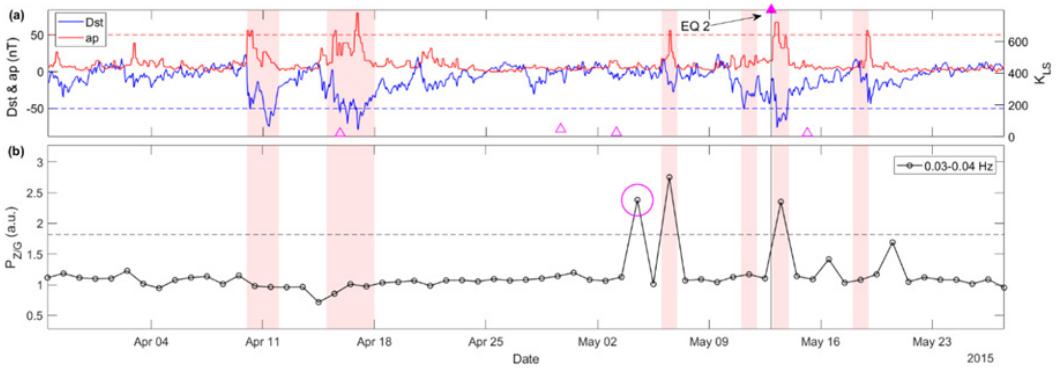

FIGURE 5. Normalized polarization ratio analysis results for EQ2. The figure shows temporal evolutions of (a) Dst and ap indices (left) and K_{LS} of earthquakes (right), and (b) $P_{Z/G}$ in 0.03 – 0.04 Hz. Dashed lines in (a) are the disturbed day thresholds, while in (b), they are the $\mu + 2\sigma$ threshold.

TABLE 2. Characteristics of the observed anomalies preceding the main earthquakes obtained using the classic and normalized polarization ratio analysis methods

EQ	Method	Date of appearance	Lead time (days)	Δf (Hz)	Amplitude (a.u.)	$\mu + 2\sigma$ threshold (a.u.)	Ratio
1	Classic	08/09/2009	22	0.04 – 0.05	2.33	1.73	1.35
	Normalized	26/09/2009	4	0.08 – 0.09	2.20	1.47	1.50
2	Classic	29/04/2015	13	0.03 – 0.04	0.59	0.55	1.07
	Normalized	04/05/2015	8	0.03 – 0.04	2.38	1.82	1.31

compared to the normalized method for EQ1 (2.33 versus 2.20); however, this was because the background value was also larger. Hence, the ratio of the amplitude to the corresponding $\mu + 2\sigma$ threshold calculation is appropriate to fairly compare the obtained anomalies from the two methods. Based on the values stated in Table 2, the ratio was larger when the normalized method was implemented for both earthquakes (i.e., 1.50 versus 1.35, and 1.31 versus 1.07), indicating that the anomalies had greater distinction.

From these two case studies, better reliability and effectiveness of the normalized $P_{Z/G}$ parameter in detecting ULF precursor were demonstrated. The parameter for both earthquakes: (1) exhibited anomality only before the mainshock, and (2) was consistently low throughout the period except on a date preceding the earthquake, making it easy for the anomaly to be distinguished. Therefore, it is suggested that the anomalies on 26th September 2009 and 4th May 2015 were possible precursors to EQ1 and EQ2, respectively.

CONCLUSION

In this study, the polarization ratio analysis method, which has been used by multiple prior studies in detecting ULF geomagnetic earthquake precursor, was further improved. This was accomplished by introducing the range type normalization process as opposed to the z-score type that was used by Ida et al. (2008). Dissimilar ranges of normalization for the vertical and horizontal geomagnetic field components were chosen, giving a larger proportion to the vertical component since the vertical component is more affected by earthquake-related underground activities. We determined that the ranges of [1, 2] for the horizontal component and [1, 3] for the vertical component maximized the reliability and effectiveness of the method. The normalized analysis method successfully identified possible precursors of two past earthquakes that occurred in Indonesia and Japan, which demonstrated the method's capability in identifying earthquakes' precursors in the equatorial and mid-latitudinal regions. It was found that the normalized method was more reliable and effective compared to the non-normalized classic method in detecting precursors, which is given by two precursor characteristics: (1) the precursor appeared only before the mainshock with no random fluctuations during other periods, and (2) the precursor had a very high amplitude relative to the background, making it easily observable.

DECLARATION OF COMPETING INTEREST

None.

ACKNOWLEDGEMENT

The authors would like to extend their gratitude to the International Center for Space Weather Science and Education, Kyushu University for providing the MAGDAS geomagnetic data. The work of Akimasa Yoshikawa is supported by MEXT/JSPS KAKENHI Grant 15H05815. The global geomagnetic indices data were obtained for free from the GSFC/SPDF OMNIWeb interface at omniweb.

gsfc.nasa.gov, while the earthquake data were obtained from the European-Mediterranean Seismological Centre from the online earthquake cataloging service at www.emsc-csem.org.

REFERENCES

Chauhan, V., Singh, O. P., Pandey, U., Singh, B., Arrora, B. R., Rawat, G., Pathan, B. M., Sinha, A. K., Sharma, A. K., & Patil, A. V. 2012. A search for precursor of earthquakes from multi-station ULF observation and TEC measurements in India. *Indian Journal of Radio Space* 41: 543–56.

Chen, C. H., Lin, C. H., Wang C. H., Liu, J. Y., Yeh, T. K., Yen, H. Y., & Lin, T. W. 2015. Potential relationships between seismo-deformation and seismo-conductivity anomalies. *Journal of Asian Earth Sciences* 114:327–37.

Currie, J. L., & C. L. Waters. 2014. On the use of geomagnetic indices and ULF waves for earthquake precursor signatures. *Journal of Geophysical. Research: Space Physics* 119 (2): 992–1003.

Dudkin, F., Rawat, G., Arora, B. R., Korepanov, V., Leontyeva, O., & Sharma, A. K. 2010. Application of polarization ellipse technique for analysis of ULF magnetic fields from two distant stations in Koyna-Warna Seismoactive Region, West India. *Natural Hazards and Earth System Sciences* 10 (7): 1513–22.

Hasbi, A. M., Ali, M. A. M., & Misran, N. 2011. Ionospheric variations before some large earthquakes over Sumatra. *Natural Hazards and Earth System Sciences* 11 (2): 597–611.

Hayakawa, M. 2015. *Earthquake Prediction with Radio Techniques.* Singapore: John Wiley & Sons Pte Ltd.

Hayakawa, M., Kawate, R., Molchanov, O. A., & Yumoto, K. 1996. Results of ultra-low-frequency magnetic field measurements during the Guam Earthquake of 8 August 1993. *Geophysical Research Letters* 23 (3): 241–44.

Hirano, T., & Hattori, K. 2011. ULF Geomagnetic changes possibly associated with the 2008 Iwate–Miyagi Nairiku Earthquake. *Journal of Asian Earth Sciences* 41 (4-5): 442–49.

Ida, Y., Yang, D., Li, Q., Sun, H., & Hayakawa, M. 2008. Detection of ULF electromagnetic emissions as a precursor to an earthquake in China with an improved polarization analysis. *Natural Hazards and Earth System Sciences* 8 (4): 775–77.

Molchanov, O. A., & Hayakawa, M. 1995. Generation of ULF electromagnetic emissions by microfracturing. *Geophysical Research Letters* 22 (22): 3091–94.

Molchanov, O. A., & Hayakawa, M. 2008. *Seismo Electromagnetics and Related Phenomena: History and Latest Results.* Tokyo: Terrapub.

Rawat, G., Chauhan, V., & Dhamodharan, S. 2016. Fractal dimension variability in ULF magnetic field with reference to local earthquakes at MPGO, Ghuttu. *Geomatics, Natural Hazards and Risk* 7 (6): 1937–47.

Rostoker, Gordon. 1972. Geomagnetic indices. *Rev. Geophys.* 10 (4): 935–50.

Serita, A., Hattori, K., Yoshino, C., Hayakawa, M., & Isezaki, N. 2005. Principal component analysis and singular spectrum analysis of ULF geomagnetic data associated with earthquakes. *Natural Hazards and Earth System Sciences* 5(5): 685–89.

Takla, E. M., Yumoto, K., Liu, J. Y., Kakinami, Y., Uozumi, T., Abe, S., & Ikeda, A. 2011. Anomalous geomagnetic variations possibly linked with the Taiwan earthquake ($M_w = 6.4$) on 19 December 2009. *International Journal of Geophysics* 2011 (2): 1–10.

Yumoto, K., & MAGDAS Group. 2007. Space weather activities at SERC for IHY: MAGDAS. *Bulletin of the Seismological Society of America* 35: 511–22.

Yusof, K. A., Hamid, N. S. A., Abdullah, M., Ahadi, S., & Yoshikawa, A. 2019a. Assessment of signal processing methods for geomagnetic precursor of the 2012 M6.9 Visayas, Philippines earthquake. *Acta Geophysica* 142:93.

Yusof, K. A., Abdullah, M., Hamid, N. S. A., & Ahadi, S. 2019b. On effective ULF frequency ranges for geomagnetic earthquake precursor. *Journal of Physics: Conference Series* 1152:1–8.

Zelinskiy, N. R., Kleimenova, N. G., Kozyreva, O. V., Agayan, S. M., Bogoutdinov, S. R., & Soloviev, A. A. 2014. Algorithm for recognizing Pc3 geomagnetic pulsations in 1-S data from INTERMAGNET equatorial observatories. *Izvestiya, Physics of the Solid Earth* 50 (2): 240–48.